JOURNAL OF THERMOPHYSICS AND HEAT TRANSFER
Vol. 18, No. 4, October–December 2004

Radiation of Spalled Particles in Shock Layers

Chul Park*
Eloret Corporation, Sunnyvale, California 94087
and
George A. Raiche II† and David M. Driver†
NASA Ames Research Center, Moffett Field, California 94035

The behavior of solid particles ejected into a shock layer from an ablating carbonaceous heat shield is investigated theoretically in order to explain the results of an experiment conducted in an arc-jet facility. The experiment found that a laser beam made to pass through the shock layer over an ablating flat-faced model is attenuated in the shock layer. The likely cause of the attenuation is the presence of solid carbon particles due to spallation. The equation of motion of the solid particles, accounting for their vaporization, is integrated for different combinations of size and ejection velocity. The assumed quantity of ejected particles and the distributions of the size and ejection velocity are varied until the calculated pattern of laser-beam attenuation matched the experimental data. The radiative heat flux reaching the wall is calculated to be up to 170 W/cm^2 in the arc-jet experiment. If this phenomenon occurs also during the entry flight of the Stardust vehicle, the wall-heating rates are predicted to be up to 8% greater than without radiating carbon particles in the shock layer.

Nomenclature

C_d = drag coefficient
D = diameter of model, cm
d_r = median initial particle diameter [Eq. (14)], μm
f_m = mass distribution function; Eq. (13)
I = intensity of laser beam, W
J = wavelength-integrated intensity, W/(cm$^2 \cdot$ sr)
M = spallation rate, g/(cm$^2 \cdot$ s)
m = initial mass of a particle, g
m_r = median initial particle mass, g
p = stagnation pressure, atm
q_c = convective heat flux to wall at stagnation point, W/cm^2
q_{cr} = convective + radiative heat flux to wall at stagnation point, W/cm^2
q_p = radiative heat flux to wall due to particles, W/cm^2
q_t = total heat flux, $q_{cr} + q_p$, W/cm^2
Re = Reynolds number
T_a = equivalent particle temperature [Eq. (10)], K
T_p = Temperature of particle, K
u_∞ = freestream velocity, cm/s
v = ejection (initial) velocity of a particle, cm/s
v_r = median ejection velocity, cm/s
W = $\int$ (vaporization rate) dy, g/(cm$^2 \cdot$ s)
x = distance along light path, cm
y = distance normal to wall, cm
α = projected area per unit volume (= extinction coefficient), cm^{-1}
β = mass distribution parameter; Eq. (13)
γ = ejection (initial) velocity distribution parameter; Eq. (15)
Δ = shock layer thickness, cm
θ = polar angle (Fig. 3)
ρ_∞ = freestream density, g/cm^3
ρ_s = density of particle, g/cm^3
σ = Stefan–Boltzmann constant
τ = projected area fraction; Eq. (8)

Presented as Paper 2004-1349 at the AIAA 42nd Aerospace Sciences Meeting and Exhibit, Reno, NV, 4–8 January 2004; received 5 February 2004; revision received 20 May 2004; accepted for publication 21 May 2004.

*Senior Research Scientist; currently Professor, Department of Aerospace Engineering, Korea Advanced Institute of Science and Technology, Daejeon 305-701, Republic of Korea; cpark216@kaist.ac.kr. Fellow AIAA.
†Research Scientist. Member AIAA.

Introduction

As a part of an ongoing effort in research on and development of thermal protection systems for planetary entries, a series of experiments was conducted recently with ablating models in an arc-jet facility at NASA Ames Research Center.[1] The tested models were made of a type of carbonaceous heat-shield material named PICA (phenolic impregnated carbon ablators). During the experiments, two types of optical measurement were made within the shock layer over the ablating model: a laser-beam-attenuation measurement and a spectral-emission measurement. The laser-attenuation measurement found that a beam of a He–Ne laser passing through the shock layer is attenuated by the shock layer when ablation occurs. The spectral-emission measurement found that continuum radiation is emitted over the entire observed wavelength range when ablation occurs.[1]

Physics of gas radiation does not explain these optical results: there are no known absorption mechanisms for the possible gas species in the ablation-product gas that can produce the observed attenuation at the laser wavelength or the emission of the continuum. The most likely explanation of the observed phenomena is the presence of small solid carbon particles ejected from the ablating wall through the so-called spallation or microspallation process. This phenomenon has been studied theoretically or experimentally in Refs. 2–7. But the new experiment is the first optical measurement of this phenomenon.

If this possible radiation by the carbon particles is substantial, it must be accounted for in the design of the heat shield for future entry vehicles. The purpose of the present paper is to extract as much information on this radiation from the new optical results.

Experiment

Because the details of the experiment are reported in Ref. 1, only the results pertinent to the present work will be summarized here.

The experiment was made in the Interaction Heating Facility of Ames Research Center, which incorporates a segmented-constrictor arc heater and operates at a maximum continuous rated power input of 60 MW. All tests were made under one operating condition of the arc heater at an electrical-input power level of 29 MW. The test gas was dry air, plus about 7% by mass of argon. It is customary

Table 1 Summary of four tested conditions

Parameter	Condition 1	2	3	4
Nozzle exit diameter, cm	30.5	15.2	15.2	15.2
Effective nozzle area ratio	42	10	10	10
Pitot impact pressure, atm	0.16	0.66	0.66	0.66
Model base diameter, cm	10.2	10.2	5.08	2.54
Effective nose radius, cm	16.0	16.0	8.0	4.0
Fay–Riddell q_c, W/cm^2	566	1050	1450	2100
Copper calorimeter q_c, W/cm^2			1150	1630
Measured recession rate, mm/s	0.1	0.2	0.4	0.8

to add argon of such a quantity in an arc-jet facility in order to increase electrical conductivity. The pressure in the plenum chamber was 4.5 atm under this operating condition. The enthalpy was determined by four different methods. The heat balance and the sonic-throat method both resulted in an average enthalpy value of 28.8 MJ/kg. The rate of heat transfer to a copper calorimeter at the stagnation point of a flat circular disk, with an uncertain surface catalytic efficiency, gave the lower limit of the centerline enthalpy as 30.5 MJ/kg. By analyzing the spectrum of the radiation emitted by the shock layer, the enthalpy value was determined to be 40.6 ± 1.4 MJ/kg. A computational fluid dynamics calculation gave the centerline enthalpy as 41.0 MJ/kg (Ref. 8).

Two different nozzles were used: one with an exit diameter of 15.2 cm and the other with a 30.5-cm exit diameter. Based on a pitot impact pressure measurement, the effective area ratios at the location of the tested models for these two nozzles were judged to be 10 and 42, respectively. The tested models were in the shape of a circular flat disk with rounded corners. The base diameter of the model, D, was varied as 2.54, 4.08, and 10.2 cm. The tests were made under four different combinations of model sizes and nozzle area ratios. The operating conditions were identified in Ref. 1 as conditions 1–4. Table 1 summarizes the operating environments of these four conditions.

The spectral emission measurements are also described in Ref. 1. The radiation power emitted by the shock layer is collected from the sideview position, over a wavelength range from about 400 to 900 nm, with a wavelength resolution of 4.5 nm. An interesting aspect of this measurement is that continuum radiation was found in the region ahead of the shock layer over an ablating model. The spectrum of this radiation was approximately that of a black body at about 3800 K, and later in this paper is attributed to the glowing solid particles. This near-blackbody radiation was visible to an observer. The radiation seemed almost one-dimensional. That is, the distance from the model surface to the edge of this near-blackbody radiation was nearly constant over most of the model diameter.

Laser-beam attenuation measurement, also described in detail in Ref. 1, was made for both copper models and ablating models. For the copper model, the laser beam is directed to cross the shock layer at a predetermined path approximately 3.2 mm away from the model surface. For the ablating models, two different approaches are made. For conditions 3 and 4, the laser beam is directed at the beginning of the test toward the side of the model a few millimeters downstream of the unablated surface of the model. For these tests, therefore, the laser beam was initially blocked. As the model ablates, the flat surface recedes, and, at a certain moment, the laser beam is cleared to pass across the shock layer.

For conditions 1 and 2, the surface recession rate was too small for this method to be applied. Therefore, the laser beam was directed initially to pass a path approximately 1.6 mm away from the model surface. For all four conditions, the output from the radiation detector varied smoothly with time as the model surface receded by ablation.

In Fig. 1, the laser-beam transmission data are summarized. For conditions 3 and 4, the attenuation trace spans the region from the model wall to beyond the shock wave. One surprising feature in the attenuation pattern is that there is no bend in the attenuation curve; that is, the slopes in these curves are continuous across the shock

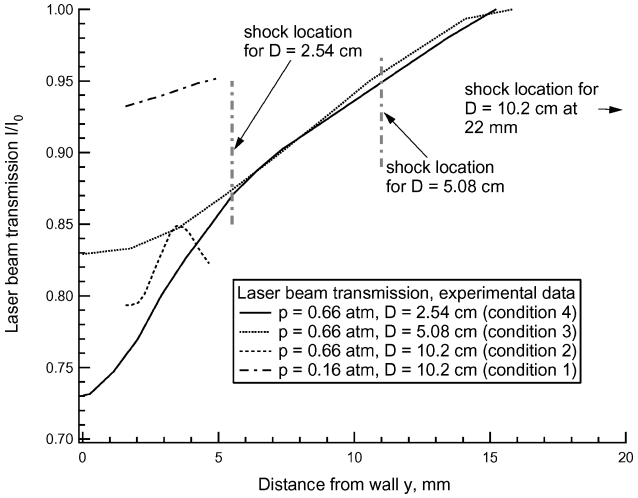

Fig. 1 Laser-beam transmission data.

wave. A particle ejected from the ablating wall travels against the flow by its inertia. For large or fast particles, the initial momentum is sufficiently large so that they travel beyond the shock wave. The drag exerted on the particle increases severalfold across the shock wave. If the drag coefficient were the same across the shock wave, the drag should increase across the shock by the density ratio across the shock. Increased drag forces the particles to turn back toward the wall. This should cause the concentration of the particles to decay more rapidly with distance in the supersonic region than in the subsonic region. This should produce a change in the slope of the attenuation curve.

The slowing in the supersonic region will be relatively more prominent for slow particles. The observed continuity of the slope in the attenuation curve implies that the speed of the particles is higher than a certain critical value. This point will be exploited in the analysis described below to extract information on the mass and ejection speed of the particles.

For conditions 1 and 2, the attenuation pattern spans only a short distance because surface recession was small. The attenuation pattern for condition 2 has an apparent reversal of the slope. This abnormal phenomenon may be attributed to the exceptional nature of this condition: the model diameter of 10.2 cm for this condition may be too large for a nozzle diameter of 15.2 cm. The enthalpy of the flow may be substantially different over the radius of the model. The central region is heated first, and the particles are ejected from the region. The outer region is heated later, and the particles are ejected there later, or vice versa. Such phenomena will produce the observed reversal of the attenuation pattern. This anomaly for case 2 is ignored; it is surmised that its impact will probably be small.

Interpretation of Experimental Data

Radiative Transfer in Particle-Laden Gas Medium

Figure 2 illustrates the process of attenuation of the laser beam through a gas medium laden with small particles. Assume first that there is only a small number of those particles within a unit cube, taken here, for illustrative purposes, to be $1 \times 1 \times 1$ mm. The laser beam is blocked by these particles. Each particle has a certain cross-sectional area. The sum of all those cross-sectional areas in the cube will be designated α:

$$\alpha = \text{projected area per unit volume} \tag{1}$$

The unit of α is mm^{-1}, or, in cgs units, cm^{-1}. The intensity I_0 of a laser beam entering this cube will be attenuated by αI_0 when it exits from the cube. If this particle-laden medium extends a thickness of Δx, the laser intensity is reduced by $\alpha I_0 \Delta x$, as indicated in the figure. Thus, the intensity of the laser beam satisfies the differential equation

$$(\text{laser beam}) \frac{\mathrm{d}I}{\mathrm{d}x} = -\alpha I \tag{2}$$

The quantity α thus becomes the so-called extinction coefficient for the laser beam.

If there is no incident laser beam, but the particles are at an elevated temperature T_p, each particle will produce blackbody radiation of (spectrally integrated) intensity J of $\sigma T_p^4/\pi$, in the units of W/(cm$^2 \cdot$ sr), assuming that the emissivity of the particles is unity and the particle diameter is sufficiently larger than the wavelength of radiation. At the end of a distance Δx, the intensity of this radiation will be $\alpha\sigma T_p^4 \Delta x/\pi$. Therefore, this intensity satisfies the differential equation

$$\text{(particle radiation)}\ \frac{\mathrm{d}J}{\mathrm{d}x} = \frac{\alpha\sigma T_p^4}{\pi} - \alpha J \tag{3}$$

The second term in this equation accounts for the blockage by the particles. The solution to this equation can be obtained easily. For the case where α times the overall path length is small, that is, optically thin, the second term in Eq. (3) can be neglected and the solution becomes approximately

$$J \approx \int_0^x \frac{\alpha\sigma T_p^4}{\pi}\,\mathrm{d}x \tag{4}$$

In order to simplify the analysis, a one-dimensional approximation of the particle-laden shock layer flow is introduced here, as shown in Fig. 3. As shown, the concentration of the particles, and consequently α, is assumed to be uniform in the direction parallel to the ablating surface and varies only in the normal direction y. This one-dimensional representation is based on the visiual observation that the distance from the model wall to the edge of the luminous particles is approximately constant, as mentioned earlier. The span

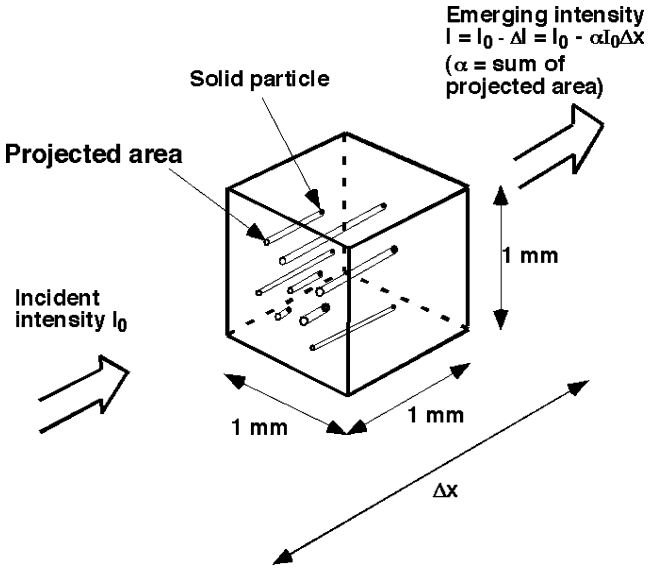

Fig. 2 Attenuation of radiation in a particle-laden gas medium.

of this regime is D, the diameter of the ablating model. The maximum extent of this regime in the y direction is Δ. Then the laser transmission across this one-dimensional shock layer is

$$I/I_0 = \exp(-\alpha D) \tag{5}$$

The intensity of radiation produced by the particles in the direction θ (Fig. 3), when α is small, is

$$J \approx \int_0^{\Delta} \frac{\alpha\sigma T_p^4}{\pi\cos(\theta)}\,\mathrm{d}y \tag{6}$$

The radiative heat flux due to this radiation, q_p, is obtained by multiplying Eq. (6) by $\cos(\theta)$ (to account for the inclination of the wall with respect to J), multiplying also by $2\pi\sin(\theta)$ (to account for the conical nature of the radiating region), and integrating over θ from zero to $\pi/2$. The result, if D is much larger than Δ and the particle cloud is optically thin, is

$$q_p \approx 2\sigma \int_0^{\Delta} \alpha T_p^4\,\mathrm{d}y \tag{7}$$

If T_p is constant, Eq. (7) reduces to

$$q_p \approx 2\sigma T_p^4 \int_0^{\Delta} \alpha\,\mathrm{d}y$$

The integral of the projected area,

$$\int_0^{\Delta} \alpha\,\mathrm{d}y$$

is a dimensionless quantity representing the fractional projected area of the particles on the wall and will be termed here total projected-area fraction and denoted by τ:

$$\tau = \int_0^{\Delta} \alpha\,\mathrm{d}y \tag{8}$$

In terms of τ, the radiative heat flux q_p is, for the case of $T_p =$ constant

$$q_p \approx 2\sigma T_p^4 \tau \tag{9}$$

According to Eq. (9), if τ is unity, q_p becomes twice the blackbody flux. This contradiction arises from the assumption of optical thinness. In reality, when τ approaches unity, the neglected blockage effect, represented by the second term in Eq. (3), suppresses the heat flux value, so that q_p approaches the blackbody value. The quantity τ is analogous to the optical depth in a gas, and therefore can be considered to be the optical depth of the particle-laden medium.

If q_p and τ are known independently, the T_p value satisfying Eq. (9) can be determined. This T_p value will be called equivalent particle temperature, and will be denoted by T_a:

$$T_a = (q_p/2\sigma\tau)^{\frac{1}{4}} \tag{10}$$

For conditions 3 and 4, τ can be determined by integrating the α values determined from the experimental values of transmission,

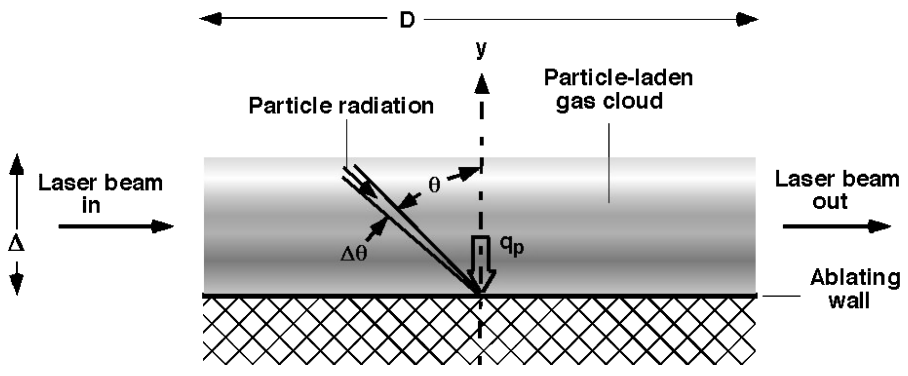

Fig. 3 One-dimensional depiction of the particle-laden shock-layer flow.

I/I_0, using Eq. (5). The τ values thus calculated are 0.0297 and 0.0740 for conditions 3 and 4, respectively. For these small values of τ, the optically thin approximations, Eqs. (4–9), are valid. If the temperature of the particles T_p were 3800 K, the particle temperature ahead of the shock wave determined experimentally in Ref. 1 (see the Experiment section) throughout the flowfield, then the radiative heat flux q_p is determined from Eq. (9) to be 63.2 and 158 W/cm^2, respectively, for conditions 3 and 4.

If the gas medium is also radiating, there will be an interaction of the gas radiation and particle radiation. For the optically thin case under consideration, this interaction will be small, and therefore is neglected.

To determine q_p more precisely, one must know the particle temperature T_p as a function of y. To do so, one must characterize the behavior of individual particles, as is done below.

Nature of Spalled Particles

Behavior of a solid carbon particle produced by spallation is studied theoretically in Refs. 2 and 7. By assuming the flowfield to be one-dimensional, as shown in Fig. 3, one needs to account only for the motion in the y direction.

Though little is known of the parameters and characteristics of these particles, certain parameters can be estimated. They are as follows:

1) The particles are spherical. Liquid droplets attain a spherical shape because of the surface tension. The spherical shape is also the favored shape for solid particles at high temperatures because the strong annealing process causes the solid particles to behave almost as a liquid droplet.

2) The density of perfect graphite is about 2 g/cm^3. The density of each particle, ρ_s, is taken here to be 1 g/cm^3, because these particles had insufficient time to be graphitized.

3) In the subsonic region in the shock layer, the drag coefficient of a particle is determinable by the use of the Stokes approximation,

$$C_d = 24/Re$$

where the Reynolds number Re is determined from the radius of the particle. The viscosity is evaluated by $\mu = 2 \times 10^{-4}(T/300)^{0.75}$ P. The effective temperature T is taken to be the algebraic average between the particle temperature T_p and the local gas temperature. Typically, for a particle of diameter 20-μm, Re is about 2 in the shock layer for conditions 2–4. For Reynolds numbers below about 2, the flow enters into a free molecular flow, and so the Stokes equation is not valid. For this reason, the maximum value of C_d is forcibly limited to 10. For large-Reynolds-number cases, the minimum C_d is forced to be 1.0, slightly larger than the sphere value in a laminar flow. Admittedly, this method introduces uncertainty of a significant extent into C_d (estimated to be on the order of a factor of 1.5). But this is still the best possible at this time.

4) In the supersonic region in front of the shock wave, the Newtonian approximation gives $C_d = 1$.

5) The collision of an oxygen atom with the solid carbon particle produces a molecule at CO through the process

$$\mathrm{O} + \mathrm{C(s)} \rightarrow \mathrm{CO} + 3.74\ \mathrm{eV} \tag{11}$$

The probability of this surface reaction is known to be 0.63 $\exp(-1160/T_p)$ (Ref. 9).

6) The collision of a nitrogen atom with the solid carbon particle produces a molecule of CN through the process

$$\mathrm{N} + \mathrm{C(s)} \rightarrow \mathrm{CN} + 0.35\ \mathrm{eV} \tag{12}$$

The probability of this surface reaction is approximately 0.3 (Ref. 10).

7) A heated solid-carbon particle vaporizes mostly into C_3. The vaporization process is described using the vapor pressure[11] and the vaporization coefficient.[12]

8) The particles are ejected from the wall in general at all angles θ. Because the velocity component parallel to the wall surface is irrelevant, all particles are assumed to be ejected normally from the wall.

9) For small particles, a free molecular approximation can be used in evaluating the heat transfer due to convection and surface-chemical reactions. However, when the controlling Knudsen number is not large, one must account for the continuum effect. The continuum effect is accounted for in the present work by dividing the free molecular values by $\sqrt{(1 + Re)}$, where Re is the Reynolds number based on the radius and the average value of the viscosity at the wall of the particles and the surrounding flow.

10) In calculating the radiation power emitted by the particles, the emissivity is assumed to be unity.

The general form of the equations of conservation of mass, moment, and energy is given in Ref. 7, and will not be repeated here. It is to be noted here, however, that particle temperature T_p is determined entirely by the balance between the heat inflow and outflow. Therefore it is a function only of the thermodynamic state of the flow, and is independent of the size or velocity of the particle.

Solid Particle Characterization

Even with the foregoing assumptions and approximations, the distribution of the sizes and initial velocities and the number of the particles are unknown. At the least, the specification of the size and initial velocity requires two parameters each: one parameter representing the median or representative value and the other representing its distribution with respect to size (or mass). Thus, there are five parameters to be determined.

From the laser-beam attenuation pattern for conditions 3 and 4, four parameters can be extracted: 1) the attenuation value at $y = 0$, 2) the distance y where attenuation disappears ($I/I_0 = 1$), 3) the value of I/I_0 at a y midpoint, and 4) the fact that there is no bend in the attenuation curve across the shock wave. Extraction of these four features is equivalent to assigning four points on the attenuation curve.

An a priori assumption is made that the mass of the particles varies by a factor of 100 between the smallest and the largest. The smallest and the largest masses are taken respectively to be 1/10 and 10 times the median mass m_r:

$$0.1m_r < m < 10m_r$$

Under this assumption, several different forms of distribution functions for both particle size and initial velocity were tried. For each candidate distribution function, the calculated extinction pattern was compared with the experimental data. The best-matching form of the mass-distribution function (the number of particles with mass m g within 1 g of the particle ensemble) was found to be

$$f_m \propto m^{-\beta}, \qquad 1 < \beta < 2$$

By imposing the condition that the integral $\int f_m m\, \mathrm{d}m$ from $0.1m_r$ to $10m_r$ is 1 g, one obtains

$$f_m = \frac{2 - \beta}{10^{2-\beta}(1 - 0.01^{2-\beta})m_r^2}\left(\frac{m_r}{m}\right)^{\beta} \tag{13}$$

The diameter of the particle having the mass m_r will be defined as the median diameter d_r, that is, that which satisfies the relation

$$m_r = \tfrac{4}{3}\pi(d_r/2)^3\rho_s \tag{14}$$

Likewise, an appropriate form of the velocity distribution function is found to be

$$v = v_r(m/m_r)^{\gamma} \tag{15}$$

where v_r is the median velocity corresponding to the median-sized particles.

Thus the particle-size and -velocity characterization introduces four arbitrary parameters, d_r, v_r, β, and γ. By adding the rate of spallation, that is, the mass of spalled particles ejected per 1 cm^2 of

ablating wall per second, M, there are five unknown parameters to be determined.

The particle ensemble is represented by 59 discrete sets of m and v values selected at equal intervals on the logarithmic scale.

Particle-Trajectory Calculation

The trajectory of each of the 59 representative particles is integrated numerically, accounting for deceleration due to drag and vaporization by the aforementioned mechanisms, in a manner described in Ref. 7. Because only the y component of particle motion is to be determined, the flowfield along the stagnation streamline is sufficient. The stagnation streamline solution is obtained using a viscous shock layer (VSL) method incorporating an up-to-date thermochemical description.[13,14] The trajectory calculation yields the size and cross-sectional area of the particle, the rates of removal of O and N and production of CO, CN, and C_3, the energy removed from the flow for these processes, and the radiation power emitted by the particle, at each y point. By multiplying these quantities by the distribution function f_m and summing, the ensemble-integrated values were obtained at each y point. The vaporization rate is calculated from the rate of production of CO, CN, and C_3. The rate of vaporization integrated over y is calculated and denoted W:

$$W = \int_0^{\Delta} (\text{vaporization rate})\, \mathrm{d}y, \ \text{g/(cm}^2 \cdot \text{s)} \qquad (16)$$

The sum of the cross-sectional area for each particle gives the extinction coefficient α as a function of the distance y. Using Eq. (5), the transmission of the laser beam I/I_0 is calculated as a function of y. Using Eq. (7), the radiative heat flux due to particles, q_p, is calculated. The I/I_0 so calculated is compared with the experimental data for conditions 3 and 4. The five parameters are varied to determine the best match with the experimental data.

Because there are five unknown parameters and only four constraints, one parameter can be chosen arbitrarily. This one arbitrary parameter is taken to be the median diameter d_r. For arbitrarily chosen d_r, a set of M, v_r, β, and γ that reproduce the experimental data can be found, as long as d_r is within a certain limit.

Generally, a small d_r requires a large v_r in order to satisfy the condition that the calculated I/I_0 agrees with the experimental data. This is understandable: as a small particle moves outward from the wall, it slows down relatively fast because drag force has a comparatively larger impact on its motion; to travel the same distance, the initial velocity must be higher. For a fast particle, the sudden increase in drag across the shock wave does not show much change in I/I_0 because the fractional change in velocity is small. Conversely, a large particle requires a small velocity. A slow particle suffers a large relative change in deceleration across the shock wave. This trend is shown in Figs. 4a and 4b.

In Figs. 4a and 4b, the stairstep appearance of the calculated result is due to the finiteness of the number of sample particles, 59. For $d_r = 10\ \mu$m (Fig. 4a), there is no discernible bend in the attenuation curve. For $d_r = 40\ \mu$m (Fig. 4b), there is. This bend occurs for d_r greater than about 20 μm.

For $d_r = 10\ \mu$m (Fig. 4a), the matching spallation rate is $M = 8.4 \times 10^{-5}$ g/(cm$^2 \cdot$ s). For $d_r = 40\ \mu$m (Fig. 4b), the corresponding value is 2.5×10^{-4} g/(cm$^2 \cdot$ s). That is, a large d_r accompanies a large spallation rate. In the absence of any experimental evidence regarding d_r, the worst case, that is, the largest spallation rate consistent with the observed laser extinction, is chosen in the present work. It is with $d_r = 20\ \mu$m. For both $d_r = 10$ and 40 μm, $\beta = 1.5$ and $\gamma = 0.15$ are valid.

The possible impact of choosing other values of d_r is shown in Figs. 5a–5c for condition 3. Figure 5a shows that M and d_r vary significantly but W varies little with the chosen d_r.

Figure 5(b) shows τ and q_p. Both τ and q_p are nearly independent of d_r. In Fig. 5c, particle temperature T_p is shown as a function of y for $d_r = 10$ and 40 μm. As seen here, there is a discontinuity across the shock wave. This is expected: the particle temperature T_p is determined by the balance between the rates of heating and cooling of the particle. Both these rates change across the bow shock wave.

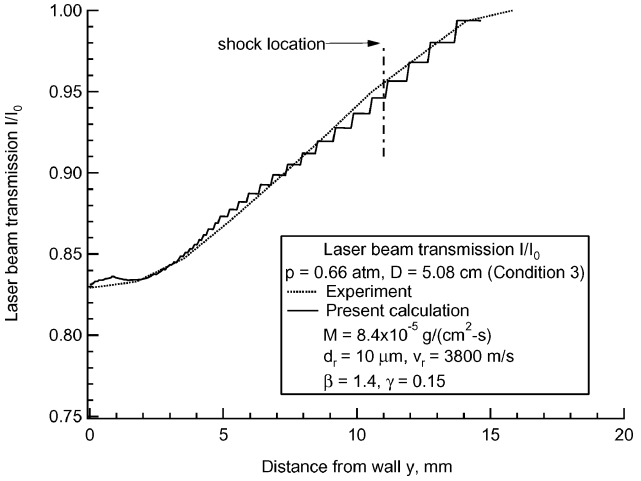

a) $d_r = 10\ \mu$m

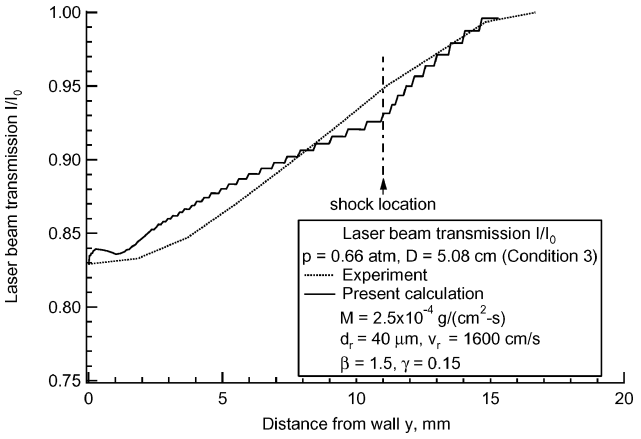

b) $d_r = 40\ \mu$m

Fig. 4 Comparison of calculated and measured laser-beam transmission patterns for condition 3.

However, as the figure shows, the difference in T_p between the two cases is small. It is to be noted that the particle temperature values calculated for the two d_r values in front of the shock wave are both close to the experimental value of 3800 K. This is an experimental validation of the present procedure.

In Figs. 6a–6d, the calculated transmission patterns are compared with the experimental data, assuming $d_r = 20\ \mu$m, $\beta = 1.5$, and $\gamma = 0.15$. Fair agreement is seen between the calculation and the experimental data.

Heat Flux Due to Particles

Results for Arc-Jet Test

Table 2 summarizes the results of the calculations made with $d_r = 20\ \mu$m, $\beta = 1.5$, and $\gamma = 0.15$. For the purpose of comparison, the freestream flow rates $\rho_\infty u_\infty$ are given in the table. The VSL values given in the table are calculated using an up-to-date method given in Refs. 13 and 14 and account for the convective and radiative blockage caused by ablation. The VSL values are smaller than the Fay–Riddell values because of the blockage effects. As seen in the table, the spallation rates M are less than 330 ppm of the freestream flow rate. The vaporization rates W are an order of magnitude smaller than the spallation rate. This means that most of the solid particles do not vaporize before they fall back to the ablating wall. The vaporization rates are less than 18 ppm of the freestream flow rate. The relative magnitudes of W with respect to $\rho_\infty u_\infty$ are less than the concentration of carbon dioxide in the test gas or in natural air. Thus, it can be said that the particles do not affect the thermodynamic state of the shock-layer flow to any significant extent.

Table 2 Summary of the calculations for the arc-jet test condions

Parameter	Condition 1	2	3	4
$\rho_\infty u_\infty$, g/(cm^2 · s)	0.329	1.272	1.272	1.272
Spall rate M, g/(cm^2 · s)	2.85×10^{-5}	8.00×10^{-5}	1.50×10^{-4}	4.20×10^{-4}
Vaporization rate W, g/(cm^2 · s)	3.77×10^{-6}	1.44×10^{-5}	1.41×10^{-5}	2.25×10^{-5}
Median velocity v_r, cm/s	1240	1750	2480	3510
Total projected area fraction τ, calc	0.00435	0.02354	0.0310	0.0760
Total projected area fraction τ, meas			0.0297	0.0740
Radiation flux q_p, W/cm^2	8.31	54.5	72.9	168
Equivalent particle temperature T_a, K	3600	3779	3793	3735
VSL-calculated q_{cr}, W/cm^2	410	771	1120	1710

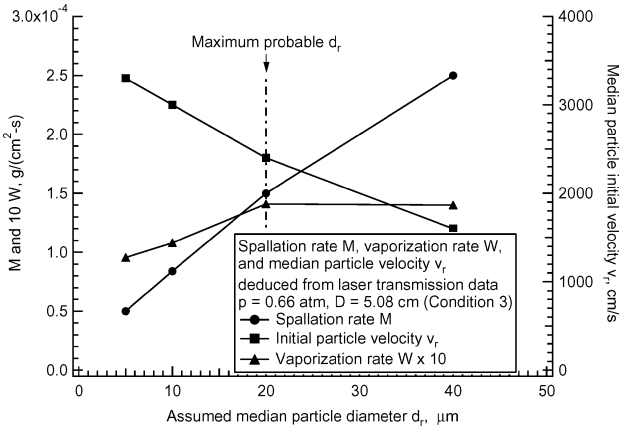

a) Spallation rate M, integrated vaporization rate W, and median initial velocity v_r

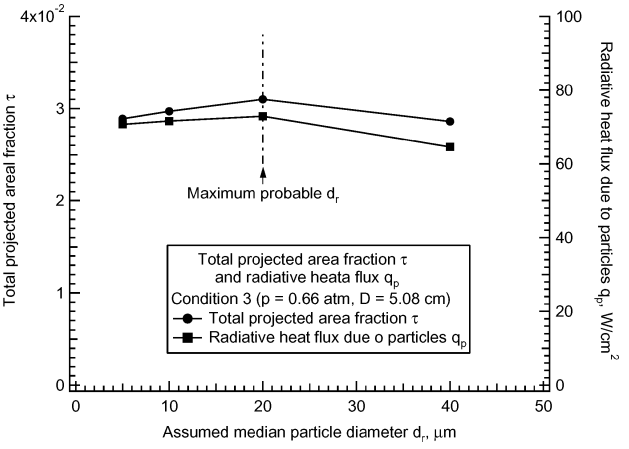

b) Total projected area fraction τ and radiative heat flux due to particles q_p

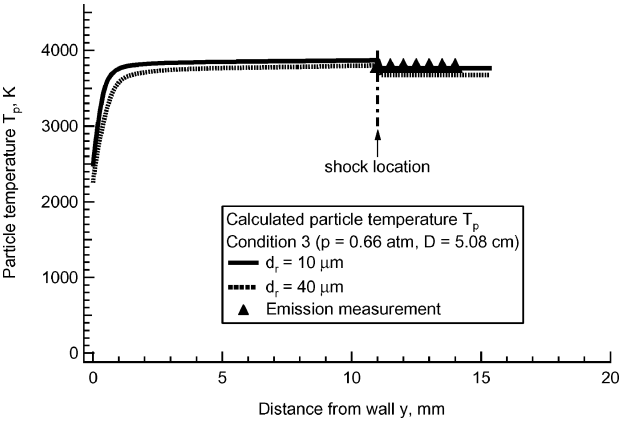

c) Particle temperature T_p

Fig. 5 Impact of assumed d_r.

Table 3 Effect of particles for Stardust entry vehicle at the stagnation point[a]

Time, s	q_t, W/cm^2	$\rho_\infty u_\infty$, g/cm^2 · s	M, g/cm^2 · s	W, g/cm^2 · s	τ	q_p, W/cm^2
42	720	.0516	6.51^{-5}	0	0.0047	7.8
48	1000	0.127	1.09^{-4}	6.92^{-6}	0.0373	70.5
54	1220	0.261	1.57^{-4}	1.30^{-5}	0.0439	93.1
60	1040	0.427	1.17^{-4}	1.61^{-5}	0.0274	58.8
66	700	0.574	6.25^{-5}	5.36^{-6}	0.0127	25.6
76	220	0.699	4.69^{-7}	3.16^{-8}	.00012	0.21

[a]The total heat flux q_t is that from Olynick et al.[15]

The calculated total projected-area fraction τ for conditions 3 and 4 agrees closely with the values determined directly from the measurement (see the Radiative Transfer in Particle-Laden Gas Medium section).

The equivalent particle temperature T_a is between 3600 and 3800 K. The temperature values are not much different from the measured value of 3800 K in the region ahead of the shock wave. The q_p values are 72.9 and 168 W/cm^2 for conditions 3 and 4, which are not much different from the estimates of 63.2 and 158 W/cm^2 made earlier (see the section Radiative Transfer in Particle-Laden Gas Mixture); the new values are at most only about 15% different from the estimates.

The spallation rate M and the ejection velocity v_r can be surmised to depend mostly on the heating rate of the wall. In Fig. 7, these two parameters are plotted against the total wall heating rate $q_t = q_{cr} + q_p$ (again with $d_r = 20$ μm, $\beta = 1.5$, and $\gamma = 0.15$). The calculated values are fitted by the cubic polynomials

$$M = -2.659 \times 10^{-5} + 1.607 \times 10^{-4}(q_t/1000) - 1.006 \times 10^{-4}(q_t/1000)^2 + 7.543 \times 10^{-5}(q_t/1000)^3, \text{ g/(cm}^2\text{-s)} \quad (17)$$

$$v_r = 1446 - 1710(q_t/1000) + 3316(q_t/1000)^2 - 969(q_t/1000)^3, \text{ cm/s} \quad (18)$$

It should be noted here that these expressions are applicable only to the PICA material tested.

Application to Stardust Flight

In Ref. 15, the stagnation-point wall heating rates are predicted for the entry flight of the Stardust vehicle. The heatshield material on the vehicle was the same PICA that was tested in the present work. Using the results of the present work, one can estimate how much radiative heat flux will be produced by the particles at the stagnation point. The total heating-rate values calculated in Ref. 15 are applied in Eqs. (17) and (18) to determine M and v_r. The calculation outlined earlier is carried out to determine the radiative heat flux q_p produced by the particles. The results of this calculation are presented in Table 3.

As seen in the table, the calculated radiative heat fluxes due to particles, q_p, are at most about 8% of the total heating rate values obtained by Olynick et al.[15]

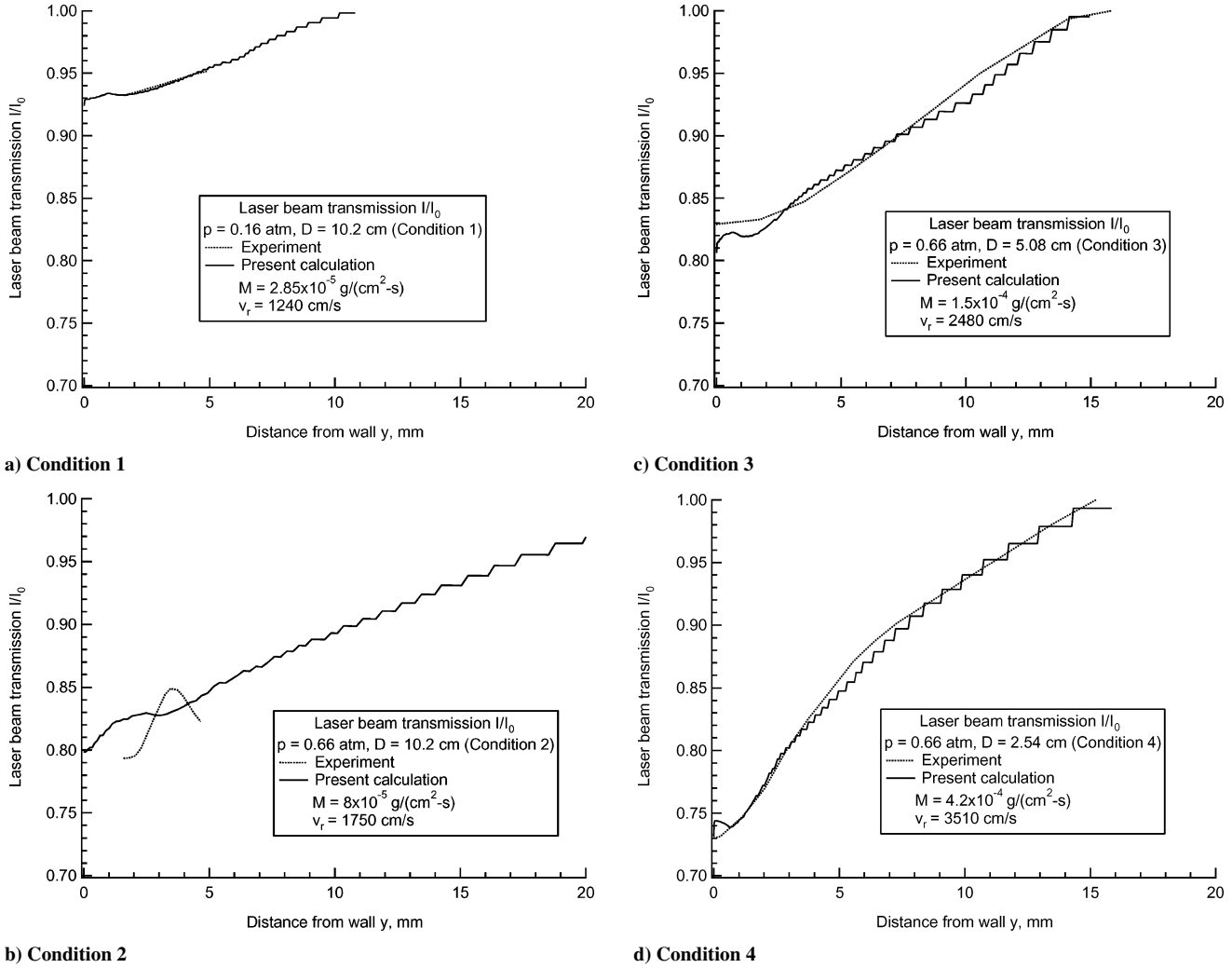

Fig. 6 Comparison between the calculated and measured laser-beam transmission.

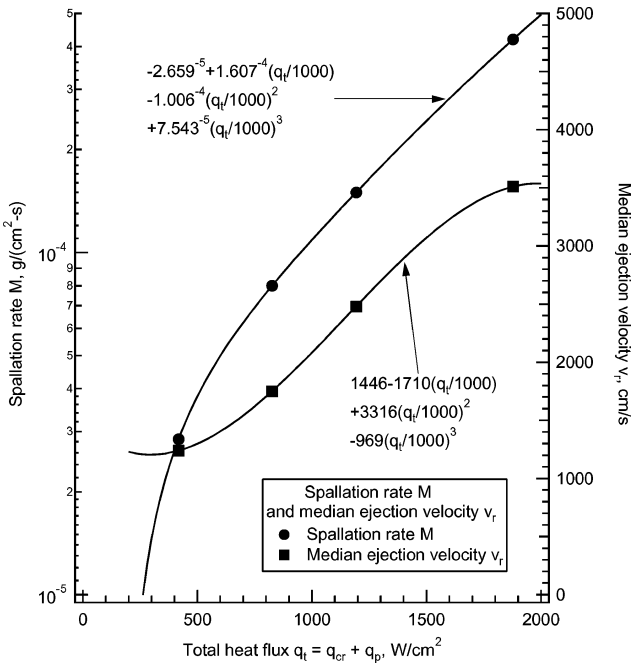

Fig. 7 Spallation rate M and median ejection velocity v_r as a function of the wall-heating rate q_c.

Discussion

The radiative heat flux produced by the spalled particles q_p is estimated initially from elemental reasoning from the measured laser-beam-attenuation pattern and the measured blackbody temperature of the particles. The detailed calculation performed in the present work yielded values of q_p that are different from the initial estimates by no more than 15%. This seemingly makes the detailed calculation almost redundant. However, conversely, this is a validation of the present detailed calculation procedure.

The detailed calculation also yielded several pertinent information. First, the calculation showed that the particle temperature does not vary greatly through the shock layer, at least in the range of conditions encountered. This is because T_p is determined mostly by the sublimation phenomenon, which is dictated by the vapor pressure of C_3: particles cannot exist at higher temperatures because they would vaporize. The next important finding of the detailed calculation is that, within the range of conditions of typical Earth entry, the spallation phenomenon does not affect the thermodynamic conditions of the shock-layer flow.

Three major assumptions have been made in the present work. The first major assumption is the combination of the 10 assumed parameter values regarding the nature of the spalled particles (see the section Nature of Spalled Particles). These assumptions are made to enable the calculation of the particle temperature T_p. As mentioned, T_p is insensitive to most of these parameters. Therefore, these 10 parameter values are relatively inconsequential.

The second of the important assumptions is that the median diameter of the spalled particles, d_r, is 20 μm, the largest probable value.

As seen in Figs. 5a and 5b, the values of d_r smaller than 20 μm would make little difference in the heat flux q_p or the amount of gaseous species produced, W.

The third major assumption is the one-dimensional representation of the particle-laden flow, illustrated in Fig. 3. Over the central half of the surface of the flat disk, the one-dimensional representation is probably valid. However, over the outer half of the flat surface, the approximation is probably poor: the wall-heating rate may be lower or higher than in the central region and, consequently, the spallation rate may be lower or higher there. If the average spallation rate over the outer half of the ablating surface were half or twice the value in the central half, then the one-dimensional model used in the present work would introduce an error on the order of a factor of 1.5 in the calculated results. Thus, one should assume the q_p value derived in the present work to be valid to within an estimated error margin of a factor of 1.5. It may be hoped that this uncertainty can be reduced in the future by carrying out a two-dimensional study: that is, two-dimensional laser-beam attenuation measurement across positions away from the flow centerline and corresponding two-dimensional theoretical analysis.

Conclusions

The pattern of attenuation of a laser beam across the shock layer over an ablating PICA model tested in an arc-jet facility can be reproduced numerically by assuming that the particle size and ejection velocity distribution are a simple power of the particle mass. The largest probable median size of the particles is 20 μm. Assuming the median size to be 20 μm, the dependence of the rate of spallation and ejection velocity is deduced from the arc-jet experiment. The radiative heat flux produced by the particles is calculated, partly supported by the experimental evidence, to be up to about 170 W/cm^2. When applied to the entry flight of the Stardust vehicle, the radiative heat flux due to particles is predicted to be up to about 8% of the total heat flux at the stagnation point, to within an estimated uncertainty margin of a factor of 1.5.

Acknowledgments

The first author acknowledges the support provided by NASA Ames Research Center through Contract NAS2-99092 to Eloret Corp. The authors also express sincere thanks to Joseph Olejniczak and Imelda Terrazas-Salinas of NASA Ames Research Center and Jan Heinemann of Eloret Corp. for providing various information used in the present work.

References

[1]Raiche, G. A., II, and Driver, D. M., "Shock Layer Optical Attenuation and Emission Spectroscopy Measurements During Arc Jet Testing with Ablating Models," AIAA Paper 2004-0825, Jan. 2004.

[2]Davies, C. B., and Park, C., "Trajectories of Solid Particles Spalled from a Carbonaceous Heat Shield," *Entry Vehicle Heating and Thermal Protection Systems: Space Shuttle, Solar Starprobe, Jupiter Galileo Probe*, edited by P. E. Bauer and H. E. Collicott, Vol. 85, Progress in Astronautics and Aeronautics, AIAA, New York, 1983, pp. 472–495.

[3]Lundell, J. H., and Dickey, R. R., "Response of Heat-Shield Materials to Intense Laser Radiation," AIAA Paper 78-0138, Jan. 1978.

[4]Park, C., "Stagnation-Point Ablation of Carbonaceous Flat Disks, Part 2: Experiment," *AIAA Journal*, Vol. 21, No. 12, 1983, pp. 1748–1754.

[5]Laux, T., Auweter-Kurtz, M., Wegmann, T., Morino, Y., Yoshinaka, T., Park, C., and Speckmann, H. D., "Comparison of Ablation Material Tests in a Plasma Wind Tunnel and Laser Heating Facilities," 3rd European Workshop on Thermal Protection Systems, Noordwijk, The Netherlands, March 1998.

[6]Yoshinaka, T., "Spallation Measurement at the Ablator Plasma Wind Tunnel Tests," National Space Development Agency of Japan, NASDA-TMR-970006E, Tokyo, Feb. 1998.

[7]Park, C., "Interaction of Spalled Particles with Shock Layer Flow," *Journal of Thermophysics and Heat Transfer*, Vol. 13, No. 4, 1999, pp. 441–449.

[8]Park, C., Raiche, G. A., II, Driver, D. N., Olejniczak, J., Terrazas-Salinas, I., Hightower, T. M., and Sakai, T., "Comparison of Enthalpy Determination Methods for an Arc-Jet Facility," AIAA Paper 2004-0487, Jan. 2004.

[9]Park, C., *Nonequilibrium Hypersonic Aerothermodynamics*, Wiley, New York, 1990, p. 351.

[10]Park, C., and Bogdanoff, D. W., "Shock Tube Measurement of Coefficient of Reaction of Nitrogen Atoms and Solid Carbon: Preliminary Results" AIAA Paper 2003-0158, Jan. 2003.

[11]Leider, H. R., Krikorian, O. H., and Young, D. A., "Thermodynamic Properties of Carbon up to the Critical Point," *Carbon*, Vol. 11, No. 5, 1973, pp. 1555–1563.

[12]Baker, R. L., McDonaugh, J. M., Herr, K. C., Klingberg, R. A., Coffer, J. C., and Covington, M. A., "Carbon Vaporization Condensation Effects," Space Div./AFSC, Rept. SD-TR-84-53, Los Angeles, July 1984.

[13]Park, C., and Ahn, H.-K., "Stagnation-Point Heat Transfer Rates for Pioneer-Venus Probes," *Journal of Thermophysics and Heat Transfer*, Vol. 13, No. 1, 1998, pp. 33–41.

[14]Park, C., "Stagnation-Point Radiation for Apollo 4," *Journal of Thermophysics and Heat Transfer*, Vol. 18, No. 3, 2004, pp. 349–357.

[15]Olynick, D., Chen, Y. K., and Tauber, M. E., "Aerothermodynamics of the Stardust Sample Return Capsule," *Journal of Spacecraft and Rockets*, Vol. 36, No. 3, 1999, pp. 442–462.